AIAA 80-0360R

Aerodynamics of a Turbojet-Boosted Launch Vehicle Concept

W.J. Small* and G.D. Riebe*
NASA Langley Research Center, Hampton, Va.
and
A.H. Taylor†
Kentron International, Hampton, Va.

Results from analytical and experimental studies of the aerodynamic characteristics of a turbojet-boosted launch vehicle are presented. This launch vehicle concept depends upon several novel applications of aerodynamic technology, particularly in the area of takeoff lift and minimum transonic drag requirements. The takeoff mode stresses leading edge vortex lift generated in parallel by a complex arrangement of low aspect ratio booster and orbiter wings. Wind-tunnel tests on a representative model showed that this low-speed lift is sensitive to geometric arrangements of the booster-orbiter combination and is not predictable by standard analytic techniques. Transonic drag was also experimentally observed to be very sensitive to booster location; however, these drag levels were accurately predicted by standard far-field wave drag theory.

Nomenclature

C_D = drag coefficient = drag/qS_{ref}
$C_{D_{min}}$ = minimum drag coefficient (equal to zero-lift drag in this study)
C_L = lift coefficient = lift/qS_{ref}
C_{L_0} = lift coefficient at $\alpha = 0$ deg
C_{L_α} = rate of change of lift with angle of attack, per deg
K = drag-due-to-lift = $\partial C_D / \partial C_L^2$
L = body length
M_∞ = freestream Mach number
q = freestream dynamic pressure
S = area
S_{ref} = reference area, approximately equal to orbiter theoretical main delta wing; for full-scale concept $S_{ref} = 929$ m^2 (10,000 ft^2), for model $S_{ref} = 0.0929$ m^2 (1 ft^2)
x = coordinate direction along body axis
x_{ac} = aerodynamic center location measured from fuselage nose
α = angle of attack, deg
Δx = increment along x axis
Δy = increment along y (spanwise) axis

Introduction

NEW aerospace systems have historically depended upon research efforts which precede final system design by many years. Such is the case in the field of space transportation systems, particularly those types that will follow the current Space Shuttle. The requirements of such new systems are not at all clear, and the diversity of the many studies in this area reflect the differing opinions and solutions to perceived future needs.[1-5] Cost of operation and manufacture, flexibility and simplicity of operation, efficiency, choice of structural concept, and engine design tradeoffs are all examples of areas that influence competing designs and provide broad areas of research opportunities.

This paper will address the aerodynamic design problem of one of the more novel of the proposed concepts, the turbojet-boosted orbiter.[3,5] Theoretical aerodynamic techniques were used to optimize full-scale concepts. A wind-tunnel investigation was then conducted to test the validity of the techniques and assumptions used in the design studies.

Key features of the turbojet-boosted orbiter concept (Spacejet) are illustrated in Fig. 1. The system is completely reusable and would operate from runways in a manner much like conventional aircraft. A rocket-powered orbiter containing liquid hydrogen and oxygen propellants is supported by twin boosters during takeoff. These boosters each hold six to eight large hydrocarbon-fueled turbojet engines of the type proposed for future supersonic transports. The boosters contain the JP acceleration fuel and the heavy takeoff rolling gear which can typically weigh as much as the orbiter payload (29,500 kg). At rotation, lift forces of nearly 580,000 N (2.6×10^6 lb) must be generated by the complete vehicle, including orbiter and booster lifting surfaces and any lift component of booster thrust. After a high angle-of-attack takeoff, the vehicle accelerates on turbojet thrust to a staging Mach number near 3.5. During acceleration to this staging Mach number, a high-dynamic pressure trajectory is followed to increase thrusting capability of the turbojet engines. At staging, both boosters separate and fly back to base. At the same time, rocket engines are ignited which propel the orbiter into Earth orbit. Re-entry and landing of the orbiter is similar to present Space Shuttle operation.

It would appear that many advantages accrue from the use of turbojet boosters combined with a horizontal takeoff mode. Versatility is enhanced by the ability to take off from many different runways instead of being constrained to just one or two launch sites, as is the case for current vertical launch vehicles. Abort operations should be similar to present-day aircraft practice. The system has inherent ferry capability to distant launch sites. Offset orbital capability could be obtained through either increased booster fuel, by in-flight refueling, or by ferry flights to a runway nearer the desired orbital plane.

Key Aerodynamic Areas

The initial aerodynamic work on this concept has focused on two key areas critical to the success of the system, takeoff performance and transonic drag. Each of these areas was addressed analytically for conceptual mission vehicles carrying Shuttle-type payloads of 29,500 kg (65,000 lb) to orbit.

Presented as Paper 80-0360 at the AIAA 18th Aerospace Sciences Meeting, Pasadena, Calif., Jan. 14-16, 1980; submitted Jan. 21, 1980; revision received June 30, 1980. This paper is declared a work of the U.S. Government and therefore is in the public domain.

*Aerospace Engineer, Hypersonic Aerodynamics Branch, High-Speed Aerodynamics Division. Member AIAA.
†Project Engineer, Hampton Technical Center. Associate Fellow AIAA.

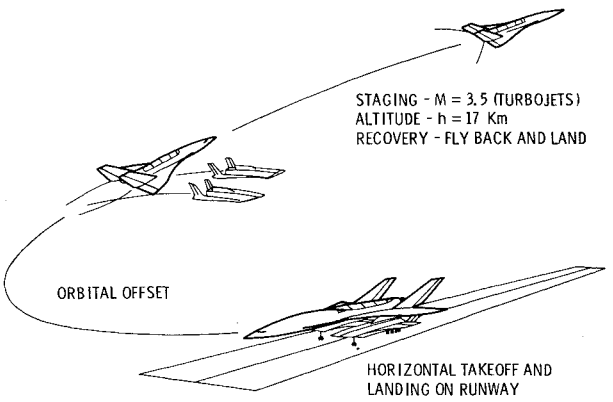

Fig. 1 Advanced space transportation concept (Spacejet).

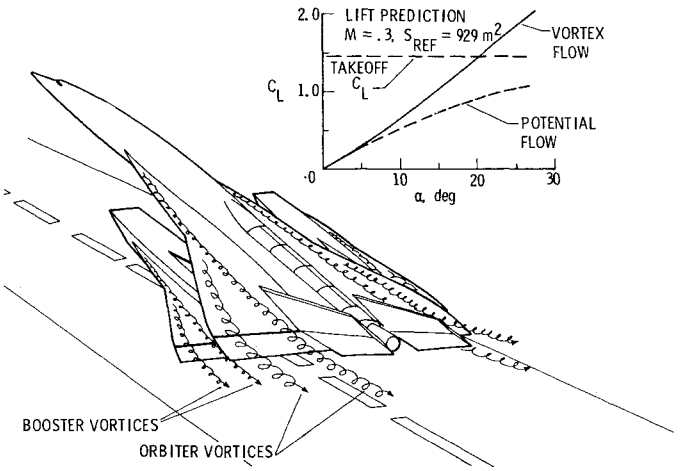

Fig. 2 Vortex lift for takeoff.

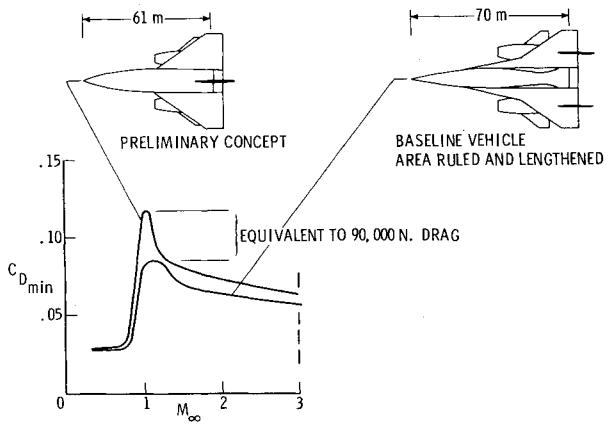

Fig. 3 Transonic drag reduction.

Low-Speed Lift

The wing of the orbiter vehicle is constrained by two factors: re-entry heating, a factor determined largely by wing loading, and by wing volume required to hold 600,000 kg (1.3×10^6 lb) of liquid oxygen. The orbiter wing contains the heavy oxidizer to minimize wing loads during taxi and horizontal flight. A wing so sized, however, does not generate sufficient lift for takeoff. The booster wings are therefore increased to the necessary planform to provide the required lift. High lift requirements also make the use of leading edge vortex lift attractive. Vortex lift occurs when flow separates from wing leading edges and forms a tightly packed set of vortices running spanwise along the wing leading edge. This vortex system entrains leeward wing flow, producing a very high-wing normal force which results in high lift and high drag at large angles of attack. High drag at takeoff is not of concern since excess thrust is available from the turbojet engines which are sized for transonic drag levels. Figure 2 illustrates, in general, the system of vortices expected from the Spacejet configuration. Lift calculations from the theory of Ref. 6 are shown on this figure and illustrate that for the baseline concept, liftoff occurs at about a 20-deg angle of attack with vortex lift. With potential flow (classical), however, sufficient lift could not be generated. If vortex lift is not utilized, then wing areas of the boosters and orbiter would have to be enlarged substantially to provide sufficient lift. For preliminary design purposes, the vortex lattice method of Ref. 6 was used for theoretical calculations with the assumption that the potential flow solution would give the correct lift when the Polhamus analogy was applied to all wing leading edges and wing tips.

A basic wing sweep of 55 deg was used primarily from leading edge heating and longitudinal stability considerations. From data presented in Ref. 7, it is clear that a 55-deg sweep wing will need a high-sweep strake ahead of the wing in order to develop lift at high angles of attack. The function of the strake is to generate a powerful leading edge vortex along the strake and over the main wing. This strake vortex generates a strong spanwise flow over the wing upper surface which in turn assists in developing and stabilizing the main wing leading edge vortex. Data from Ref. 7 show that such a strake-wing combination should provide increasing lift to angles of attack of 25 and 30 deg. At these high angles of attack, the vortex flow over the main wing breaks down at some point while the vortex flow over the strake continues to generate lift over the strake. The result can be a strong pitch-up caused by the loss of main wing lift. Maximum angles of attack during takeoff, therefore, will be constrained by the need to avoid nearing this pitchup point.

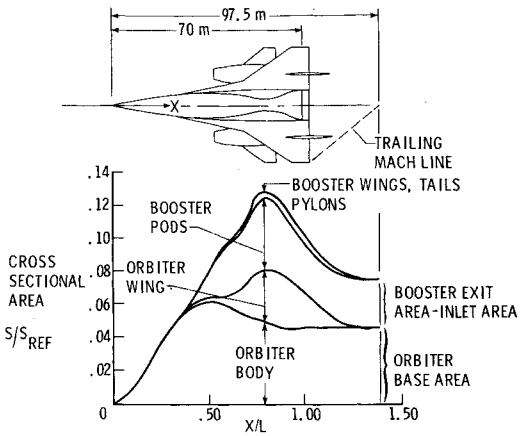

Fig. 4 Wave drag area distribution, $M = 1.3$ (full-scale concept).

Transonic Drag

Acceleration due to thrust-minus-drag forces becomes critical at low supersonic Mach numbers and becomes the determining factor in sizing the turbojet engines.[3] Drag reductions in this range have a multiplying effect on the system size since reductions in drag reduce turbojet size, which leads to both weight reductions and further decreases in drag levels due to turbojet pod size. Because of high dynamic pressures during transonic acceleration, only small angles of attack (about 4 deg) are needed to provide the necessary lift. At these low angles of attack, the most important contribution to supersonic drag is the zero-lift wave drag.

Wave drag at a particular Mach number depends upon the shape of the vehicle cross-sectional area distribution as it develops axially along the length of the orbiter-booster system.[8] The "Spacejet" type of vehicle has a large buildup of area due to the fairly thick wing (8% of chord thickness)

used to store liquid oxygen, the large orbiter fuselage, and the twin boosters. Figure 3 shows a preliminary design which had a peak $C_{D_{min}}$ near 0.12 as calculated by the method of Ref. 8. By lengthening the body about 9 m and area ruling the fuselage, peak transonic drag levels were reduced 25%, or the equivalent of 90,000 N (400,000 lb) of drag. Figure 4 shows the cross-sectional area distribution of the area ruled design at Mach 1.3. Since the cross-sectional areas are calculated from projections normal to the body axis of cutting planes parallel to the Mach angle, the total effective vehicle length is greater than the actual length for all Mach numbers greater than 1. Experience has shown that area ruling at Mach 1 (normal cross-sectional areas) may result in higher drag effects at moderate supersonic Mach numbers (near 1.3), whereas area ruling at Mach numbers such as 1.3 appears to result in overall drag reduction through the low supersonic range. In area ruling the orbiter fuselage, care was taken not to interfere with the 4.6-m (15 ft) diameter payload bay region which is similar to that of the present Space Shuttle. A large orbiter base area results from the use of three Space Shuttle-type main rocket engines. The turbojet engines of the boosters were designed with an exit area approximately twice the Mach 3 design inlet area. Since these boosters contribute considerably to the overall vehicle area, design modifications to the boosters could significantly affect wave drag forces. For purposes of wave drag calculations, the boosters were input to the program of Ref. 8 with the inlet and exit areas sized for a Mach 3 flight condition. True engine conditions at transonic speeds, however, are such that turbojets typically will not pass all the air the inlet can provide, and large inlet spillage flow can develop. Exhaust areas also close down considerably from their full open position. The resulting inlet spillage and boattail drag forces are derived from Ref. 9, and are accounted for separately as engine installation losses in mission analysis programs. The entire subject of inlet spillage and boattail drag effects is of great importance and intimately tied up with the engine cycle, inlet/exit design, and Mach number range of the vehicle. Further work on these airbreathing systems will necessarily involve a closer look at the propulsion integration problem.

A detailed breakdown of the theoretically derived drag of the full-scale vehicle is presented in Fig. 5. Wave drag dominates the overall drag, but near Mach 1, the orbiter base drag is also large and accounts for about 40% of the orbiter-alone drag and for nearly 30% of the overall orbiter plus booster drag. Clearly, methods for reducing this base drag could have large performance benefits. The two boosters account for about 35% of the total system drag. Typically, the sum of the isolated orbiter and booster drags is somewhat less than if the orbiter and booster are calculated as an integrated system, as is done here. Although not shown, the booster drag is calculated to be nearly 85% wave drag. At a Mach number of 3.5, boosters separate from the orbiter and, as shown in Fig. 5, the orbiter base drag is removed due to the ignition of the orbiter rockets.

Predictions of detailed interactions between components on a complex vehicle such as this are clearly beyond the capability of current analytical tools, particularly when one considers the many areas over which shock impingement and consequent boundary-layer separations might occur. The accuracy of generalized methods such as the far-field wave drag theory on this type of vehicle will be described in following sections.

Wind-Tunnel Model

A 1/100-scale wind-tunnel model (Fig. 6) was constructed to determine the accuracy of theoretical techniques on this class of vehicle. Unlike the full-scale concepts, the fuselage is

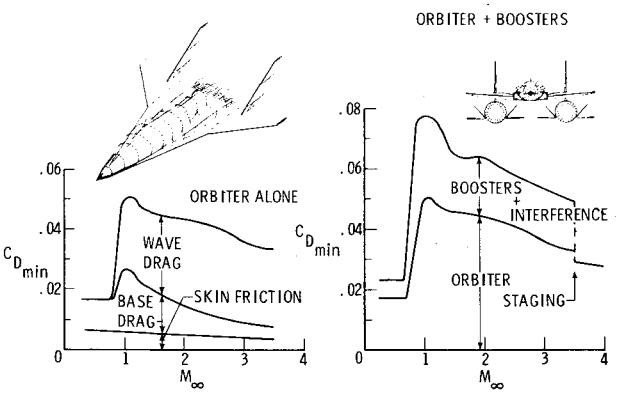

Fig. 5 Zero-lift drag breakdown (full-scale concept).

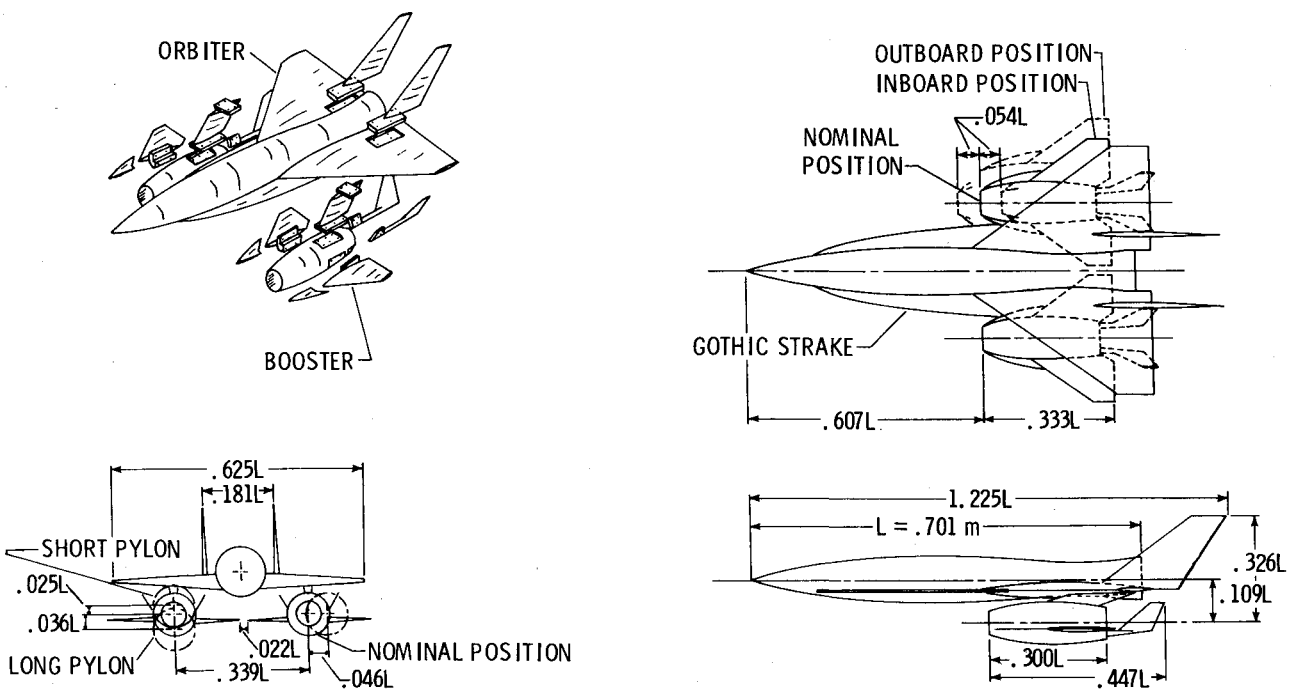

Fig. 6 Spacejet model.

of circular cross sections. It is, however, symmetrically area ruled, approximating the area distribution of the full-scale vehicle. A low, 55-deg swept delta wing can accept the boosters in a variety of positions, as shown in Fig. 6. Wing leading edges simulate a full-scale 0.15-m leading edge diameter. A number of different wing-strake designs were constructed and tested for their effect on the low-speed vortex lift characteristics of the concept. The Gothic strake shown in the figure was designed by John E. Lamar using his procedure as outlined in Ref. 10. In this method, the strake leading edge is contoured to generate a prescribed suction distribution which increases to a high value near the tip or strake-wing juncture.

Twin orbiter vertical fink sit just outboard of a possible opened Shuttle-type payload door. Twin canted booster fins were designed to provide useful longitudinal stability as well as directional control for booster-alone flight. Only limited tests were conducted with the fins in place, primarily to determine any adverse effects they may have on drag and lift.

Booster pods are of circular cross section with constant area flow-through ducts. Since the booster engine exit area is twice that of the engine, a considerable base area remains on each booster model. These base area pressures, as well as the orbiter's, are measured and corrected to freestream static pressures for all experimental data presentations in this paper. Additionally, calculated booster duct skin friction has been removed from all measured axial force.

To insure turbulent boundary layers over all model surfaces, boundary-layer trips were applied behind the fuselage nose and all leading edges. Trips were also applied inside the booster flow-through ducts.

Model tests were basically organized so as to study high angle-of-attack lift forces at low subsonic speeds, and drag forces at low angles of attack at transonic and supersonic speeds. The following test facilities were used: 1) Langley 8-ft transonic pressure tunnel, $M=0.3$-1.2; 2) Langley 7-$\times$10-ft high-speed wind tunnel, $M=0.3$; and 3) Langley unitary plan wind tunnel, $M=1.5$-2.86.

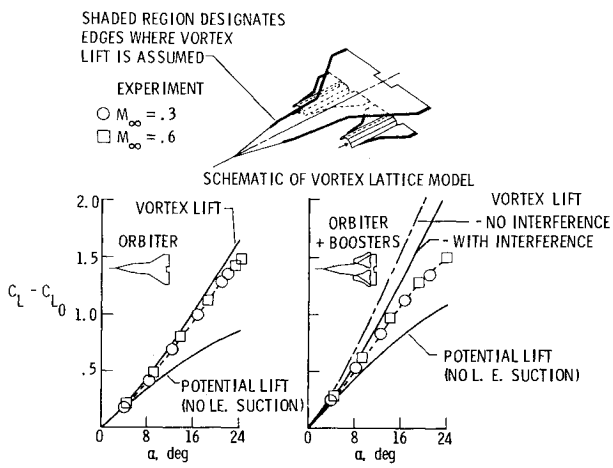

Fig. 7 Low-speed lift, nominal configuration (no fins).

Experimental Results

Low-Speed Lift Characteristics

Low-speed lift characteristics of the isolated orbiter with Gothic strakes and no fins were predicted to within 12% by the vortex lattice method of Ref. 6, as shown in Fig. 7. This vortex lattice method basically solves the potential flow problem for arbitrary planforms. The potential flow solution without leading edge suction terms is shown in the figure as a reference value. Theoretical leading edge suction forces are calculated as part of the solution, and the strength of this suction force, through the use of the Polhamus analogy, can be used to estimate wing normal forces due to leading edge vortices. Calculational procedures, such as this, require as input a description of the regions over which the vortex force is to be calculated. The vortex lattice modeling schematic shown in Fig. 7 illustrates how, in the present case, the vortex flow areas were specified. For the orbiter alone, this area consisted of strake and wing leading edges and wing side edges (tip chord).

The camber capability of the vortex lattice program was not utilized in these calculations, thus C_L at 0-deg angle of attack (C_{L_0}) was calculated identically equal to zero. Comparisons

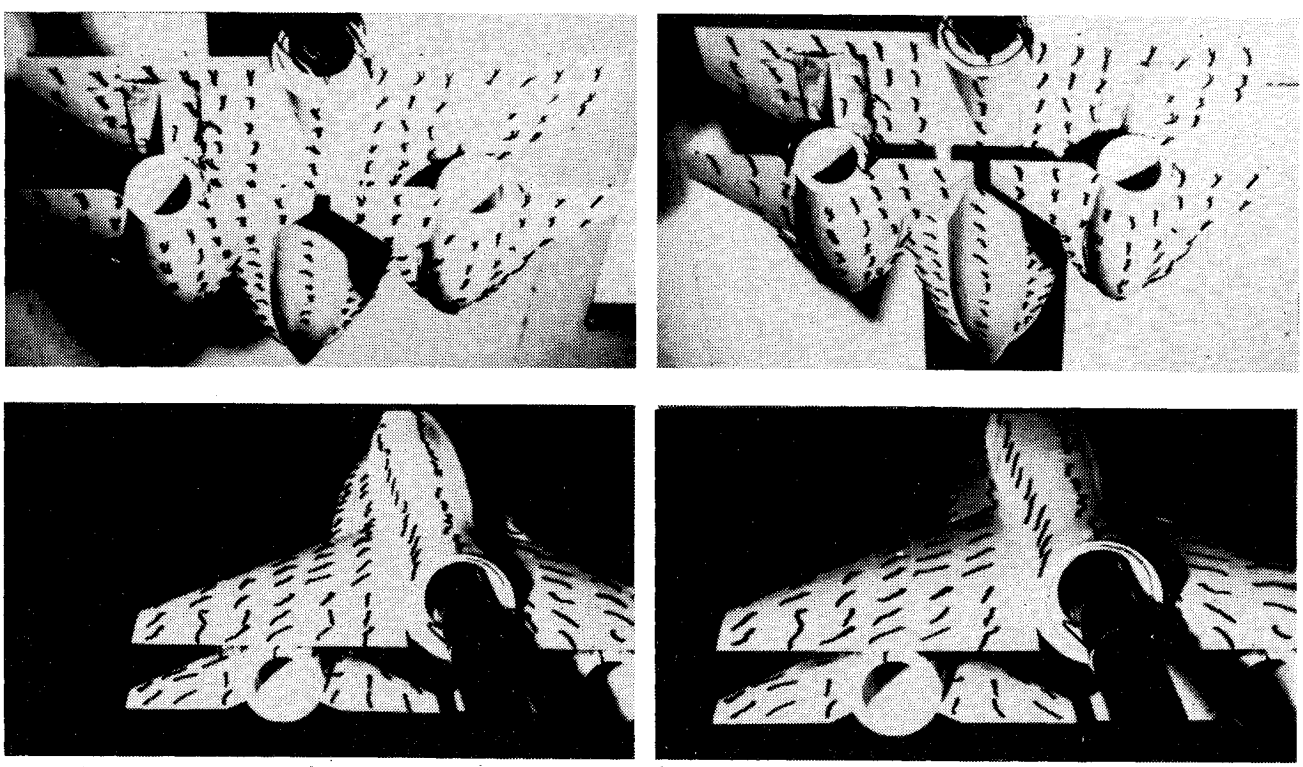

Fig. 8 Low-speed flow visualization studies, Langley 7-$\times$10 ft high-speed wind tunnel, $\alpha=12$ deg, $\alpha=12$, $\alpha=20$ deg, $\alpha=20$ deg.

with data are therefore shown as $(C_L\text{-}C_{L_0})$. For the orbiter-alone case, C_{L_0} is negligible; for the boosters-on case, C_{L_0} is fairly small and varies with booster location, as will be shown later.

The good agreement of the data with the theory for the orbiter-alone case demonstrates that substantial amounts of vortex flow are being generated by the strake-wing system. In contrast, as shown in Fig. 7, tests on the orbiter plus booster model showed lift values at 20-deg angle of attack that are 22% lower than theory predicted. Test data shown in this figure are for the boosters located inboard at a nominal fore-aft position and at nominal (middle) separation distance between booster and orbiter. The data show that the booster contributes only marginally in increasing lift. In fact, if the differences in C_{L_0} are included, the lift of the orbiter alone and the orbiter with boosters, is almost identical at $\alpha = 20$ deg.

The theoretical treatment of the model does account for about 17% loss in lift due to orbiter-booster interference. Booster input to the program of Ref. 6 attempted to account for the booster body thickness by modeling the body upper surface as dihedral and by not applying leading edge vortex flow over this area. It was felt, however, that the differences between data and theory were the result of leading edge separation effects between the orbiter and booster wing surfaces. This may be altering the assumed potential flow solution sufficiently to produce the almost complete loss of extra lift expected from the boosters.

Flow visualization tests were undertaken to try to understand the flow phenomenon over the wind-tunnel model. Tuft studies, oil flow, and smoke visualization techniques were employed to observe flowfield effects with and without the boosters and for a range of booster heights. In general, it was observed that a double set of vortices, much as was shown in Fig. 2, existed over the top of the orbiter upper surface both with and without boosters attached. As the tuft flow photographs of Fig. 8 show, there appears to be a major difference between flow over the booster inboard and outboard wing upper surfaces. At moderate angles of attack ($\approx$12 deg), the outboard wing of each booster exhibits marked spanwise flow over the upper surface, a characteristic of leading edge vortex flow. Vortex action is very weak over the booster inboard upper wing surface as evidenced by the basically streamwise flow pattern in that area. This may be caused in part by the large induced downwash angles under the orbiter body. At angles of attack near 20 deg, possibly very weak vortices developed over the inboard wings of the boosters. Flow patterns over the orbiter undersurface appear to exhibit basically streamwise patterns, as can be seen from the photographs of Fig. 8. Although it cannot be seen from these photographs, it was observed from flow observations with a tufted probe that the booster wing vortices did pass very close to the orbiter wing undersurface. It is surmised, therefore, that the lack of lift generated by the boosters represents a combination of adverse factors, principally the combination of strong downwash to the booster wings coupled with the spatial distribution of booster wing vortices between booster and orbiter wing surfaces, causing lowered pressures on both surfaces. The large booster bodies were also initially suspected as contributing to this large loss in lift. Although not shown here, tests were conducted on a flat-plate (no fuselage) representation of the booster. Results with this flat booster were very similar to that of the booster wing-body, thus implying that booster body effects were minimal in causing adverse lift interference.

Separation distance between boosters and orbiter is undoubtedly one variable affecting lift interference. In the limit, of course, as the separation distance approaches infinity, all interference effects disappear. Three pylon heights were used to vertically separate the boosters from the main orbiter. These three positions are shown in the model drawing of Fig. 6. Results from tests of several separation distances are shown in Fig. 9 for boosters mounted in the inboard nominal

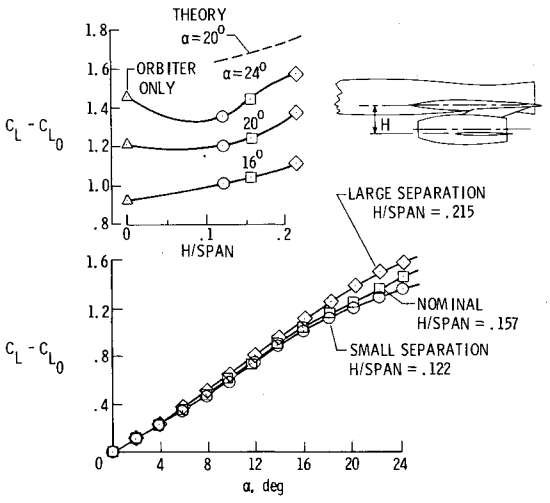

Fig. 9 Orbiter-booster seperation effects, inboard nominal position, $M = 0.3$.

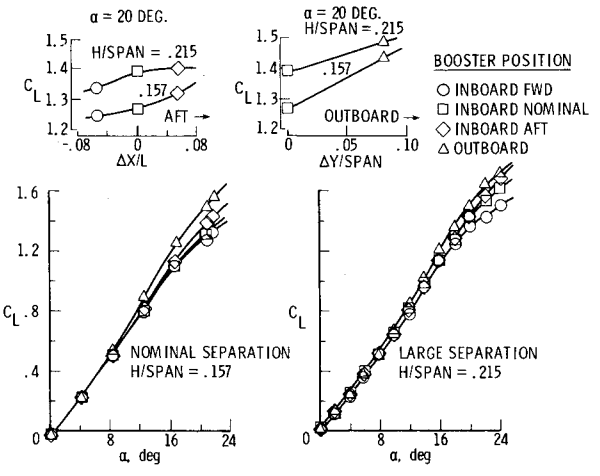

Fig. 10 Booster effects with fore-aft and outboard position $M_\infty = 0.3$ (Gothic strake).

position. As shown in this figure, the larger the separation distance, the greater the lift increase achieved. Cross plots of experimental lift data for selected angles of attack are shown on this same figure. When the theory of Ref. 6 is compared to these cross plots, the rate of lift increase with separation height is seen to be similar to experiment, although the error in magnitude is over 20%. Orbiter-alone data are used on these cross plots to represent a zero-separation height, although strictly speaking, the orbiter alone does not have as large a subtended planform as the orbiter plus nominal booster combination. Note that until large separation distances are reached, the boosters have negligible or negative influences on lift. It is expected that if the separation height were increased, increases in the combined lift values would approach the no-interference levels predicted by theory, as shown in Fig. 7. In a total system design, the increase in lift with separation height must be balanced against increased structural weight and operational problems associated with larger pylons. The difference in height between the smallest and largest pylon height tested is equivalent to about 4 m (13 ft). Further modest increases in wing plane separation height could be achieved by locating the booster wings on the bottom of the booster fuselage.

Tests were also conducted with boosters in a forward, rearward, and outboard position; these locations are shown on the model drawing of Fig. 6. Results from these experiments for two different pylon heights are shown in Fig. 10. In general, lift is improved if the boosters are moved aft

and outboard. Lift improvements occur more rapidly for the shorter pylon, but the longer pylon heights always produce greater lift. The more rearward booster locations may be influencing a smaller area of orbiter undersurface, thus increasing lift. Similarly, movement to more outboard locations may subtend less of the orbiter area and at the same time place the boosters in a more favorable downwash field. The aft-mounted and outboard booster positions at large separation heights shown in Fig. 10 are the best found during this series of tests. At 20-deg angles of attack, vehicle lift with boosters in the outboard position is increased about 12% above that of the orbiter-alone, which is still short of the design lift at $\alpha = 20$ deg by about 10%. It is interesting to note, however, that in the better booster positions, lift is increasing rapidly with angles of attack up to 24 deg. The lift of the inboard-aft boosters on the long pylons looks particularly good at these high angles and develops a lift coefficient (1.69) at 24-deg angle of attack, which is equal to the theoretically expected C_L at $\alpha = 20$ deg for the nominal booster location. This implies, then, that aerodynamic lift could be developed satisfactorily by the system if it were to rotate to 24-deg angle of attack at takeoff rather than the 20 deg which was the original goal.

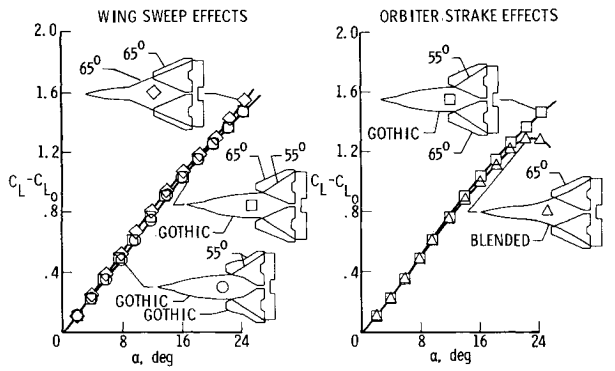

Fig. 11 Strake and leading edge effects, $M_\infty = 0.3$.

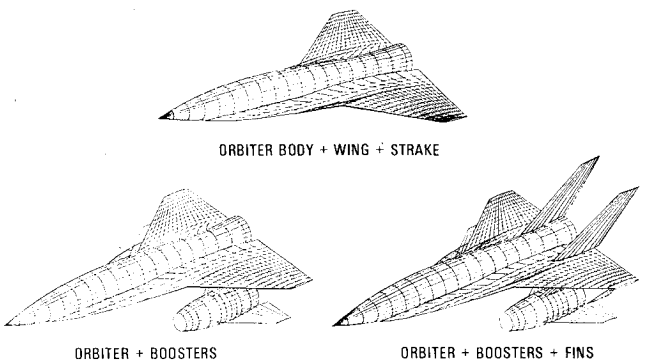

Fig. 12 Geometry input to wave drag program.

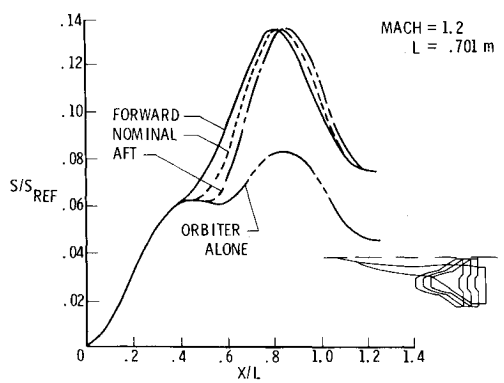

Fig. 13 Equivalent body area distribution for inboard booster locations (no fins).

Two other modifications were made to the orbiter-booster system in an attempt to gain additional lift. Wing sweep was increased from 55 to 65 deg on the boosters and orbiters, and a blended strake was interchanged for the Gothic strake on the orbiter. Both of these changes were intended to improve leading edge vortex flow strength. As seen in Fig. 11, the 65-deg booster wing showed no improvement. However, the 65-deg orbiter wing did improve overall lifting characteristics, but only because orbiter wing area was increased with this modification. Changing the Gothic strake to a blended shape resulted in a loss in lift at moderate and high angles of attack. At the highest angles, a severe pitchup problem developed with the blended strake configuration and the model began to buffet. As a result of their favorable effects, the Gothic strakes were continued as the baseline design.

Drag Characteristics

At subsonic and supersonic speeds, drag can be divided into a minimum drag at zero lift and a drag component due to lift. Because analytic techniques used in this study follow this division, the drag data will be presented as minimum drag and drag-due-to-lift. Except during the high angle-of-attack takeoff, most of the flight trajectory is a low angle-of-attack acceleration, and drag-due-to-lift is not nearly as large as is the minimum drag.

Subsonic minimum drag is calculated basically as a function of skin friction modified by form factors which account for pressure drag over wings, fuselages, and engine pods.[11]

Supersonic wave drag over the model was calculated by the far-field wave drag theory of Ref. 8, which analyzes the overall system area distribution and is not concerned with the details of local surface interaction. To use this method, the geometry must be modeled in some fashion, such as required by the computer code of Ref. 8 which calculates cross-sectional area distributions along Mach planes. A sample of the numerical geometry used in these theoretical calculations is shown in Fig. 12. All parts of the configuration are modeled with good accuracy except for booster strakes, which contribute only a negligible cross-sectional area increment, and because of program limitations are not included in the modeling.

An example of area distribution contours, calculated by this method for the numerical model without fins, is shown in Fig. 13 at a Mach number of 1.2. Minimizing drag in this Mach number range is critical to the mission concept as previously discussed, and area plots such as these provide clues as to methods of reducing this drag. Notice that as the boosters move aft, the cross-sectional area changes become more severe, and consequently increase overall drag. An inspection of the curves shows that the forward booster position produces the smoothest area distribution and could be expected to have the lowest drag if area ruling principles indeed apply to a complex configuration such as this.

Experimental results have shown surprisingly good agreement with theory. Figure 14 presents these data and theory for the model without fins. The theory consists of the wave drag analysis of Ref. 8 plus a skin friction increment calculated by the T-prime method.[12] Skin friction accounted for about 20% of the minimum drag at Mach 1.2. It is remarkable, considering the complexity of the model, how faithfully theory tracks the data. Note that an overall 20% reduction in minimum drag is realized by moving boosters forward, which is well predicted by the theory. The supersonic-area-rule theory predicts Mach number effects through changes in the shape of the area distribution curves. In general, as Mach number increases, effective maximum cross-sectional areas decrease and the area distributions tend to become smoother and subtend a greater length. Occasionally, as can be seen in the figure, the area distribution which was

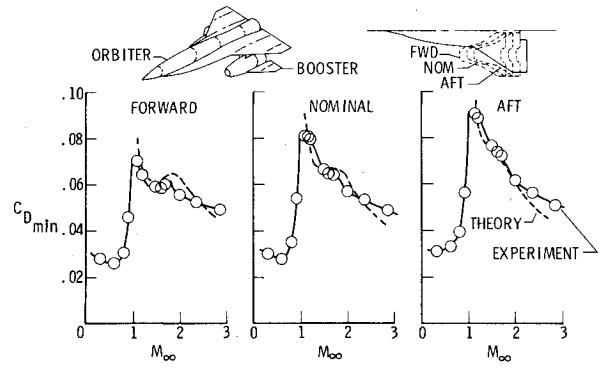

Fig. 14 Booster location effects on drag, inboard positions.

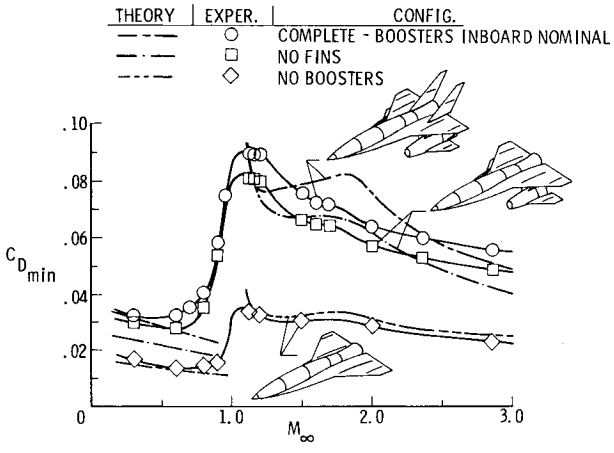

Fig. 15 Effect of configuration buildup on drag (Gothic strake).

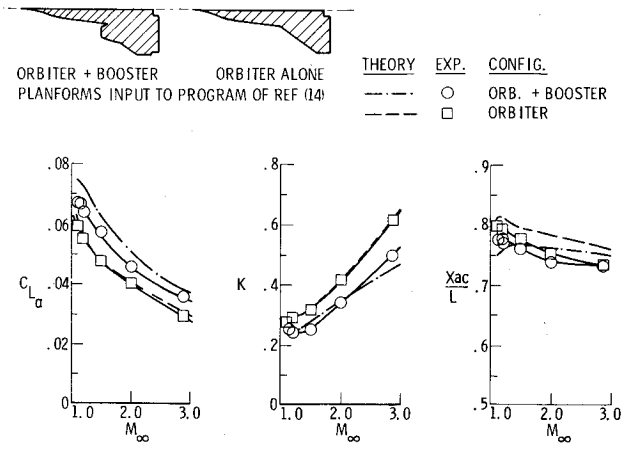

Fig. 16 Comparison of supersonic lifting surface theory with experiment ($\alpha \approx 4$ deg).

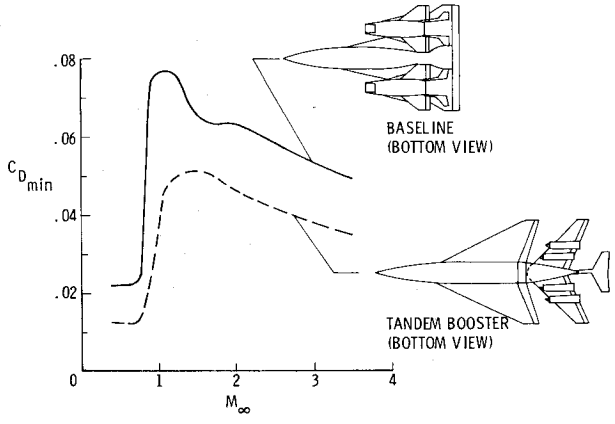

Fig. 17 Alternate turbojet-boosted orbiter concept.

near optimum for one Mach number becomes rapidly nonoptimum at higher or lower Mach numbers. In general, the agreement between theory and experiment implies that the drag of this type of vehicle is very sensitive to area ruling effects. Furthermore, these effects can be predicted and the analysis methods can be applied in system optimization during design studies.

Examination of subsonic data in Fig. 14 also illustrates that the highest drag configuration (aft booster) also exhibited the lowest drag-rise Mach number. The very low subsonic drag levels are all about the same since they are basically a function of skin friction, which will vary only slightly with booster location.

Component buildups were conducted with the wind-tunnel model and compared to experiment. Minimum drag variation with Mach number is shown in Fig. 15. Oribter-alone drag is well predicted by theory as is the booster-orbiter combination without fins (the "nominal" case of Fig. 14). Addition of fins to the orbiter-booster vehicle does cause a considerable mismatch between theory and experiment; at times the theory is high, as around Mach 1.8, and at times low, as it is at Mach 1.2. Oil flow tests were conducted on the model with the fins, and no significant regions of separated flow could be identified as being caused by the fins. Considerable flow angularity was seen in the flow impinging on these surfaces, and perhaps this flow angularity causes localized regions of constructive or destructive interference, depending on Mach number. As appears to be the case at subsonic speeds as well, the eventual design and placement of vertical stabilizers will require considerable experimental testing and will be highly dependent upon the details of the vehicle design.

Low-speed (subsonic) drag is seen to decrease with Mach number due to wind-tunnel test conditions, in which Reynolds number increased with Mach number (atmosphere stagnation pressure). From Mach 1.5 to 2.86, however, the Reynolds number is constant at 6.56×10^6/m.

Supersonic Lift Characteristics

Comparisons between the theoretical lifting surface method of Ref. 13 and angle-of-attack data at supersonic speeds are shown in Fig. 16. The upper diagram on Fig. 16 illustrates the input planform of the orbiter-booster combination. The input was an uncambered flat plate with an outline equivalent to the subtended outline of the orbiter-booster. The orbiter-alone was input similarly. Considering the simplicity of the input, agreement between theory and experiment is surprisingly good. Aerodynamic centers, for example, are predicted to within 3 or 4%. That the agreement is this close implies that in those regions where the boosters overlap the orbiter, mutual cancellation of forces occurs. It should be pointed out that data slopes were taken near 4-deg angle of attack, the likely attitude of the vehicle during acceleration. At higher angles of attack, though, the experimental pitching moment becomes nonlinear and is not well predicted by lifting surface theory as used.

Alternate Concepts

As a result of the theoretical and experimental work on the orbiter-booster design already described in this paper, several alternative concepts have suggested themselves.

One such concept, the tandem booster, is illustrated in Fig. 17. By attaching a single booster to the base of the orbiter, the large base area drag is eliminated and the effective fineness ratio of the vehicle is increased. Preliminary calculations show large reductions in drag as compared to the standard baseline concept. Possibly only half the number of turbojet will be needed for transonic acceleration, which helps further reduce the drag level. For the concept shown on Fig. 17, eight

under-over SST-type engines are mounted on a high wing. Since the engine arrangement on the booster wing precludes the use of vortex lift for this wing surface, it is assumed to develop potential flow at high angles of attack using high-lift devices.

Conclusions

1) Conceptual use of vortex lift for the turbojet-boosted orbiter concept resulted in a design allowing very high wing loading at takeoff. Booster wings were designed to supplement the main orbiter lift. Experimental tests at low speed showed strong vortex lift was generated for the orbiter design. Experimental lift with boosters attached achieved only half the increment predicted by theory; nonetheless, sufficient lift can be generated by the system to achieve satisfactory takeoff.

2) Predictions from standard supersonic drag theories were in very good agreement with experimental data for a complex vehicle having multiple bodies and wing surfaces in close proximity to one another.

3) The application of area ruling principles was found to have a very significant effect on supersonic drag. Experimental tests confirmed these theoretical results, both trendwise and in magnitude.

References

[1] Henry, B.Z. and Decker, J.P., "Future Earth Orbit Transportation Systems/Technology Implications," *Astronautics & Aeronautics*, Vol. 14, No. 9, Sept. 1976, pp. 18-28.

[2] *Proceedings of the AIAA Conference on Advanced Technology for Future Space Systems*, Langley Research Center, Hampton, Va., May 8-11, 1979.

[3] Jackson, L.R., Martin, J.A., and Small, W.J., "A Fully Reusable, Horizontal Takeoff Space Transport Concept with Two Small Turbojet Boosters," NASA TM 74087, 1977.

[4] Martin, J.A., "Use of a Duct-Burning Turbofan for an Earth-to-Orbit Vehicle Booster," AIAA Paper 79-1405, Princeton, N.J., May 14-17, 1979.

[5] Hepler, A.K., Zeck, H., Walker, W., and Scharf, W., "A Turbojet-Boosted Two-Stage-to-Orbit Space Transportation System Design Study," NASA CR-159018, April 1979.

[6] Lamar, J.E. and Gloss, B.B., "Subsonic Aerodynamic Characteristics of Interacting Lifting Surfaces with Separated Flow Around Sharp Edges Predicted by a Vortex-Lattice Method," NASA TN D-7921, Sept. 1975.

[7] Lamar, J.E. and Luckring, J.M., "Recent Theoretical Developments and Experimental Studies Pertinent to Vortex Flow Aerodynamics—With a View Towards Design," *AGARD Symposium on High Angle of Attack Aerodynamics*, Sandefjord, Norway, Oct. 4-6, 1978.

[8] Harris, R.V., Jr., "An Analysis and Correlation of Aircraft Wave Drag," NASA TM X-947, March 1964.

[9] Morris, S.J. and Foss, W.E., Jr., "Assessment of Variable-Cycle Engines for Mach 2.7 Supersonic Transports: A Status Report," NASA TM X-73977, Nov. 1976.

[10] Lamar, J.E., "Analysis and Design of Strake-Wing Configurations," *Journal of Aircraft*, Vol. 17, No. 1, Jan. 1980, pp. 20-27.

[11] Hoak, D.E., "USAF Stability and Control Datcom," Air Force Flight Dynamics Laboratory, U.S. Air Force, Oct. 1960.

[12] Monaghan, R.J., "An Approximate Solution of the Compressible Laminar Boundary Layer on a Flat Plate," British Aeronautics Research Council, R&M No. 2760, 1953.

[13] Carlson, H.W. and Middleton, W.D., "A Numerical Method for the Design of Camber Surfaces of Supersonic Wings with Arbitrary Planforms," NASA TN D-2341, June 1964.